Compensating for Elastic Deformation of the Indenter in Hardness Tests of Very Hard Materials

Roger Yu Lo and David B. Bogy
Computer Mechanics Laboratory
Department of Mechanical Engineering
University of California, Berkeley
Berkeley, CA 94720

ABSTRACT

The current method of analysis for hardness measurements by indentation is reviewed and examined. Although, the method is based on Sneddon's solution for an elastic stress field within a homogeneous half space indented by an elastically deformable indenter, it implicitly assumes a fixed indenter geometry. Therefore, if indentations are made on materials whose hardnesses are close to that of the indenter, the indenter geometry could change during the indentation process, and this method would underestimate the contact area and thus, overestimate the hardness and modulus values of the indented materials. A new method based on the Hertz contact theory is proposed. This method accounts for the indenter's elastic deformation while indenting on hard materials. The method also provides a simple way to calculate the tip radius at the origin (which will be described later). The restrictions of this method are also indicated and discussed. Finally, the hardness and modulus values for two recently developed films are measured and calculated by this method, and the results are compared with published finite-element-simulation results.

1 INTRODUCTION

The demand for higher areal storage density for disk drives has driven the development of thinner and harder protective films for disks and sliders. Nanoindentation tests have been widely adopted to study the mechanical properties, such as hardness and modulus of these films. The modified Sneddon's solution for an elastic field within a homogeneous half space indented by a solid of revolution is usually used to analyze the load/displacement curves obtained from experiments. Indenters are implicitly treated as rigid bodies by using a fixed tip shape function. (This point will be explained in detail later in this section.) When indenting on materials with hardnesses of 50GPa or lower, a diamond indenter can be treated as a rigid body and no appreciable errors will be introduced. However, if indentations are made on much harder materials, for example, the recently developed cathodic-arc amorphous carbon films, the diamond indenter deforms during the indentation processes. As the demand of harder protective films for disk drives continues, even harder materials will be developed. The current method of analysis will then fail to predict the right hardness and modulus values. A new technique is needed to compensate for the diamond indenter deformation during indentation.

The new method proposed here is based on the Hertz contact theory for elastic solids. The hardness values for the cathodic-arc amorphous carbon films calculated by this method are compared with those from Sneddon's solution and those from the finite-element simulation obtained by Follstaedt *et al.* (1997). Together with the current

method, the new method is able to estimate the indenter tip radius by a series of indentations on fused Quartz.

Indentation tests in this report were made by the Hysitron single-axis tester, which is a commercially available nanomechanical test instrument. The system is able to obtain the load-unload/displacement curves for indentations. The resolutions of the system are 0.2nm in depths and 0.1μN in forces. The software version 3.0 was used to record and to analyze the data according to Sneddon's solution. A triangle-based pyramid-shaped diamond indenter with a tip radius of about 160nm was used. Cathodic-arc amorphous carbon films were used for obtaining samples with hardness near that of diamond.

1.1 Review of the current method

The current method of analyzing the load/displacement curve is based on Sneddon's[1] solution for an elastic stress field within a homogeneous half space when it is indented by a rigid flat punch. He derived a simple relationship between the contact stiffness *S*, the projected area of indentation (or, the contact area) *A*, and the elastic modulus *E* of the indented material, i.e.

$$\frac{dP}{dh} = S = 2\sqrt{\frac{A}{\pi}}\left(\frac{E}{1-\nu^2}\right), \tag{1}$$

where ν is the Poisson's ratio of the indented material. For elastically deformable indenters, the term in the parenthesis can be generalized to the reduced modulus E_r, which is defined as

$$\frac{1}{E_r} = \frac{1-\nu^2}{E} + \frac{1-\nu_i^2}{E_i}. \tag{2}$$

Thus, Eq. (1) can be re-written as

$$S = 2\sqrt{\frac{A}{\pi}}E_r . \tag{3}$$

Pharr *et al.*[2] extended this expression to the deformation behavior of an elastic half space indented by any punch that can be described as a solid of revolution of a smooth function. Therefore, Eq.(3) can be used to analyze the load-unload/displacement curves obtained from indentation experiments with non-flat indenters. (A detailed discussion on the validity of Sneddon's solution is provided elsewhere[5].)

Among the variables in Eq.(3), the contact stiffness S can be calculated from the unloading curve for each indentation. Therefore, we have two unknowns involved in Eq. (3), the contact area A and the reduced modulus E_r. So it is an indeterminate system. The system becomes determinate if we introduce a tip shape function. The tip shape function is the relation between the contact depth and contact area, i.e. $A = A(h_c)$, which is the shape of the assumed rigid tip. The tip shape function can be found by a series of indentations on materials with homogeneous and isotropic mechanical properties, for example, fused Quartz. Since the reduced modulus of fused Quartz is known, the contact area of each indentation can be calculated from Eq. (3). According to Sneddon's solution, the contact depth can also be calculated for the same indentation. The tip shape function can thereby be established. Equation (3) together with the tip shape function constitute a closed system.

1.2 Problem associated with the current method

Finding the tip shape function on fused Quartz implicitly assumes that the tip shape is a fixed geometry. This is true if the tip is made of diamond and indentations are on relatively soft materials. For most materials used in disk drive applications, for example, silicon, silicon carbide, silicon nitride, hydrogenated carbon, nitrogenated carbon, etc., the method predicts hardness and modulus values quite well. However, if indentations are made on the recently developed cathodic-arc amorphous carbon films whose hardnesses are close to that of diamond, this method fails to predict the right hardness and modulus values. In fact, since the tip deforms to increase the contact area between itself and the indented material, this method underestimates the contact area and thus, overestimates the hardness and modulus, according to the definition of hardness and Eq.(3). A new method that accounts for indenter deformation during indentation is needed to solve the problem.

2 COMPENSATING FOR ELASTIC INDENTER DEFORMATION

2.1 Theoretical background[3]

When two solids are brought into contact, they initially touch at a single point or along a line. As the contact force increases, they deform near their points of first contact. Figure 1 shows a schematic diagram of this concept. The solids are shown as convex for convenience. They could be of any shape as long as they are topograpgically smooth. The point of first contact is taken as the origin of a rectangular coordinate system. The common tangent plane at the origin is taken as the *x*-*y* plane. The z-axis is chosen to coincide with the common normal to the surfaces at the origin. The sense of the z-axis is chosen to point to Body One. Before any interaction of these two solids, the profile of each surface near the origin can be expressed approximately in the form,

$$z = Ax^2 + By^2 + Cxy + \ldots, \tag{4}$$

where higher order terms are neglected. The separation between the two surfaces is given by

$$s = z_1 - z_2 = A_1x^2 + B_1y^2 + C_1xy - \left(A_2x^2 + B_2y^2 + C_2xy\right) = A'x^2 + B'y^2 + C'xy\,. \tag{5}$$

By properly choosing the *x*, *y* axes, we can make *C'* zero, and hence

$$s = A'x^2 + B'y^2 = \frac{x^2}{2R'} + \frac{y^2}{2R''}, \tag{6}$$

where *A'* and *B'* are positive constants and *R'* and *R''* are defined as the principal relative radii of curvature. *A'* and *B'* can be written in terms of *R'* and *R''* by,

$$A' + B' = \frac{1}{2}\left(\frac{1}{R'} + \frac{1}{R''}\right) = \frac{1}{2}\left(\frac{1}{R_1'} + \frac{1}{R_1''} + \frac{1}{R_2'} + \frac{1}{R_2''}\right), \tag{7}$$

and

$$B' - A' = \frac{1}{2}\left\{\left(\frac{1}{R'_1} - \frac{1}{R_1''}\right)^2 + \left(\frac{1}{R'_2} - \frac{1}{R_2''}\right)^2 + 2\left(\frac{1}{R'_1} - \frac{1}{R_1''}\right)\left(\frac{1}{R'_2} - \frac{1}{R_2''}\right)\cos 2\alpha\right\}^{1/2} \tag{8}$$

where R_1' and R_1'' are the principal radii of curvature of the first surface at the origin and R_2' and R_2'' are the principal radii of curvature of the second surface at the origin and α is the angle between the axes of principal curvature of each surface. If the bodies can be described as solids of revolution with respect to the origin, then $R_1' = R_1'' = R_1$ and $R_2' = R_2'' = R_2$, thus, $A' = B' = \frac{1}{2}(1/R_1+1/R_2)=1/2R$. Therefore, the separation between two surfaces can be simplified as

$$s = \frac{1}{2R}\left(x^2 + y^2\right) = \frac{r^2}{2R}. \tag{9}$$

Figure 2 shows the geometry of two solids of revolution in contact under the application of a normal load P. u_{z1} and u_{z2} are the displacements of points S_1 on surface 1 and S_2 on surface 2 due to the contact pressure. h_1 and h_2 are the displacements of distant points in the two bodies T_1 and T_2. a is the radius of the contact circle. After deformation, if the points S_1 and S_2 coincide with each other within the contact surface, then

$$u_{z1} + u_{z2} + s = h_1 + h_2 = h\,, \tag{10}$$

where h is the relative displacement of two distant points T_1 and T_2. Equation (10) has to be satisfied for all points within the contact circle, i.e. for $0 \le r \le a$.

Now, we will consider the contact of two bodies of special shapes: one is a solid of revolution (the indenter) and the other is a homogenous half space with a flat surface (the

specimen material). Thus, R_1 is the tip radius at the origin and $R_2 \to \infty$. From Eq.(9), the separation of S_1 and S_2 before deformation is

$$s = \frac{r^2}{2R_1}. \tag{11}$$

Therefore, Eq. (10) becomes

$$u_{z1} + u_{z2} = h - \frac{r^2}{2R_1}. \tag{12}$$

The pressure distribution proposed by Hertz, which results in displacements satisfying Eq. (12), is given as

$$p = p_0\left[1-\left(\frac{r}{a}\right)^2\right]^{1/2},\ r \le a, \tag{13}$$

where p_0 is the maximum pressure. Hertz also showed that the normal displacement induced by this pressure distribution is

$$u_z = \frac{1-\nu^2}{E}\frac{\pi p_0}{4a}\left(2a^2 - r^2\right),\ r \le a. \tag{14}$$

Equation (14) is valid for both bodies. Subscripts have been dropped for convenience. Therefore, Eq. (12) can be written as,

$$u_{z1} + u_{z2} = \left(\frac{1-\nu_1^2}{E_1} + \frac{1-\nu_2^2}{E_2}\right)\frac{\pi p_0}{4a}\left(2a^2 - r^2\right) = \frac{\pi p_0}{4aE_r}\left(2a^2 - r^2\right) = h - \frac{r^2}{2R_1}, \tag{15}$$

where E_r is the reduced modulus as defined in Eq.(2). Again, Eq. (16) is valid for all r smaller than a. Re-arranging Eq. (15), we have

$$h = \frac{\pi p_0}{4aE_r}\left(2a^2 - r^2\right) + \frac{r^2}{2R_1}, \tag{16}$$

where h and a are variables independent of r. Since the left hand side of Eq. (16) is not a function of r, the right hand side cannot be a function of r either. Therefore, all terms involving r on the right hand side should cancel out. Thus, we have

$$\frac{\pi p_o}{4aE_r} = \frac{1}{2R_1}, \tag{17}$$

or,

$$a = \frac{\pi p_0 R}{2E_r}. \tag{18}$$

Note that the subscript 1 of R has been dropped for simplicity. Substituting Eq. (18) back to Eq. (16), we obtain

$$h = \frac{\pi a p_0}{2E_r} = \frac{a^2}{R}. \tag{19}$$

The total load can also be calculated by integrating the pressure over the contact area, i.e.,

$$P = \int p(r) 2\pi r dr = \frac{2}{3} p_0 \pi a^2. \tag{20}$$

Substituting for p_0 by $\frac{3}{2}\frac{P}{\pi a^2}$ into Eq.(18) and Eq. (19), we have

$$a = \left(\frac{3PR}{4E_r}\right)^{1/3}, \tag{21}$$

$$h = \frac{a^2}{R} = \left(\frac{9P^2}{16RE_r^2}\right)^{1/3}. \tag{22}$$

The second equality in Eq. (22) can be re-written as,

$$P = \frac{4}{3} E_r \sqrt{Rh^3}. \tag{23}$$

Taking the first derivative of P with respect to h, we obtain

$$\frac{dP}{dh} = 2E_r\sqrt{Rh} = 2aE_r = 2\sqrt{\frac{A}{\pi}}E_r, \tag{24}$$

in which the first equality of Eq. (22) has been invoked. Equation (24) is the same as Eq. (3), which is derived from Sneddon's solution. Thus, Eq. (3) can be derived from Hertz contact theory for the elastic stress field within a homogenous half space indented by any punch that can be described as a solid of revolution of a smooth function.

The restrictions of this derivation are that the contact radius has to be much smaller than the tip radius as well as the lateral and axial dimensions of the two bodies. That is to say $a << R$, and $a << l$, where l represents the lateral and axial dimension of the bodies. These restrictions are easily satisfied in the specimen side. However, if indentations are made on the nanometer scale, care is needed in applying these equations, since the restrictions may not be satisfied. A detailed discussion will be provided in the next subsection.

2.2 Accounting for elastic indenter deformation

Equation (22) and Eq. (24), which are re-written below, constitute a determinate system for E_r and a (or A), unlike the results from Sneddon's solution, from which only Eq. (3) can be obtained.

$$h = \frac{a^2}{R} = \frac{A}{\pi R} \tag{22}$$

$$\frac{dP}{dh} = S = 2\sqrt{\frac{A}{\pi}}E_r \tag{24}$$

Equation (22) states a linear relation between the contact area A and the indenter displacement h, which can be measured experimentally, as long as R is a constant. Since

the tip radius R is defined at the origin, a constant R indicates that deformation is localized in the vicinity of the origin. Besides, there are only geometric parameters, instead of material properties, involved in Eq. (22). This means that Eq. (22) is valid for all materials with the same geometry parameters. That is to say, Eq. (22) is only tip dependent. If we can obtain the relation between the indenter displacement and the contact area on one material for a particular tip, this relation holds for all materials inasmuch as indentations are done within the restrictions.

There are two approaches for obtaining the relation between indentation depth and the contact area for a particular tip. The first one is based on a known tip radius. By substituting the tip radius into Eq. (22), we can construct the relation between the indentation depth and the contact area. The tip radius is usually estimated from SEM pictures of the region near the origin[4]. However, this is often a lengthy and expensive process. The accuracy of this method is also a concern. The second approach for getting the indentation depth and contact area relation is to indent on any homogeneous and isotropic material, for example, fused Quartz for a range of indentation depths. Contact areas can be calculated by the method mentioned in Sec. 1, since no appreciable deformation is expected if a diamond tip is used. Indentation depths can be easily read out from the load-unload/displacement curve obtained from each indentation test. Figure 3 shows the contact area vs. the indentation depth for tip 47. The curve does not look linear over the entire range (0 – 250 nm). This means that the tip radius R is not a constant within the range shown, and thus the Hertz solution is not applicable. However, if we consider only the lower part of the curve, (for example, for indentation depths lower

than 85nm), the curve can be fitted by a linear function in that range without experiencing large errors, as shown in Fig. 4. Thus, the technique based on the Hertz contact theory is valid in this range of indentation depths. This range is called the working range. After obtaining the fitted linear function for the area vs. depth curve, we can calculate the tip radius by dividing the slope of the function by π. In the case of tip 47, its tip radius with respect to the origin is 160 nm. Determining tip radii by this approach involves only a simple calculation and no special equipment is needed.

After Eq. (22) has been used for a particular tip, indentation tests can then be conducted for materials as hard as the diamond indenter. For each indentation, the maximum indentation depth can be read out from the load-unload/displacement curve. Substituting the maximum depth into Eq. (22), we can calculate the maximum contact. Thus, the hardness, which is defined as the maximum indentation force divided by the maximum contact area, can be calculated. Besides, the slope S_{max} for the unloading curve at the maximum indentation depth can be calculated by approaches discussed elsewhere[5]. Substituting S_{max} and the maximum contact area into Eq. (24), we can calculate the reduced modulus at the maximum indentation depth.

Next, we need to determine if it is sufficient to consider only the elastic deformation of the indenter. Figure 5 shows the hardness measurement of fused Quartz using tip 47 before and after indenting on a cathodic-arc amorphous carbon film (cathodic-arc DLC film) whose hardness is close to that of diamond. The hardness values were calculated by the method mentioned in Sec. 1 with the tip shape function obtained before the test, since

no significant deformation of the diamond indenter is expected while indenting on fused Quartz. The same tip shape function was used in the calculation before and after indenting. If the indenter had experienced plastic deformation or other damage during indenting on the cathodic-arc DLC film, the tip shape would have changed permanently, and so the tip shape function would have changed. However, according to the data shown, there is no significant difference in the measured hardness before and after indenting on the cathodic-arc DLC film. This indicates that the tip shape did not change permanently. Therefore, it is sufficient to consider only the elastic deformation of the diamond indenter.

2.3 Experiments

Figure 6 shows the hardness values for a cathodic-arc amorphous carbon film with a thickness of 500nm, which was deposited under –100V substrate bias. Note that the abscissa is the residual depth, instead of the indentation depth. The empty triangles represent the hardness data calculated by the method mentioned in Sec. 1. The solid triangles show the hardness data calculated by the new technique based on the Hertz contact theory. The data plotted are within the working range of the theory, i.e. the maximum indentation depths are smaller than 85nm. The values represented by the empty triangles are significantly higher than the ones represented by the solid triangles. The relatively low hardness at the film surface is due to predominant sp^2 bonding near the surface[6]. A similar phenomenon has been reported by Pharr *et al*[7].

Follstaedt *et al.*[8] have adopted a finite element technique to calculate the hardness and the modulus of this film. In their approach, they matched the finite-element-simulated load-unload/displacement curve with the experimentally found load-unload/displacement curve by varying the film elastic modulus and yield strength. The hardness they obtained was 68.4 ± 2.5 GPa at a residual depth of around 30nm. This result appears to agree with the data shown in Fig. 6. Figure 7 shows the reduced modulus values for the same film. The empty symbols also show higher values than those shown by the solid symbols. Note that the difference in the reduced modulus between these two methods is not as much as that in hardness. This is because the reduced modulus depends only on the square root of the contact area in Eq. (24), while the hardness depends on the contact area itself. Note that the values shown on Fig. 7 are the reduced modulus of the film/indenter system. Substituting the elastic parameters for diamond (E = 1140GPa and ν = 0.07) into Eq. (2), we find that $\frac{E}{1-\nu^2}$ for the film itself is about 500GPa. Assuming that the Poisson's ratio equals 0.25, we can roughly estimate the elastic modulus of the film to be 470GPa. However, the simulated result reported by Follstaedt *et al* is 848 ± 10 GPa at a residual depth of 30nm. No explanation is available at this point for the inconsistency. Figures 8 and 9 show the hardness and modulus values of a different cathodic-arc amorphous carbon film, which was deposited under –2000V substrate bias. In this case, the values represented by the empty symbols are not significantly different from those shown by the solid symbols. This indicates that if there is no deformation of the indenter, the technique based on the Hertz contact theory predicts the same hardness and modulus values as the methods mentioned in Sec. 1. The relatively low hardness values at the film surface are explained by the same argument as provided for the other film. According to the data

shown in Fig. 8, this film exhibits a hardness of 25GPa at a residual depth of 40nm, which agrees well with the value (27.5 ± 0.7 GPa) reported by Follstaedt *et al.* The elastic modulus at 40nm residual depth can be roughly estimated to be 300GPa by the same approach as mentioned above. This number is not far from the modulus (360GPa ± 10GPa) reported by Follstaedt *et al*, unlike the modulus for the film deposited under –100V substrate bias. Knapp *et al.*[9] have a detailed discussion on their simulation techniques.

3 SUMMARY AND CONCLUSIONS

Sneddon's solution can be derived from the Hertz contact theory (Eq. (24)). The relation between the contact area, indentation depth, and tip radius can be obtained (Eq. (22)). The system of equations derived from the Hertz contact theory is determinate. No extra assumption is necessary, for example, such as a constant tip shape, to close the system. Thus, the method proposed here is able to account for the indenter elastic deformation if indentations are made on materials as hard as the indenter. If a diamond indenter is used, considering only the elastic deformation is sufficient according to experimental experiences. Besides, the tip radius at the origin can also be calculated if the contact areas are known. No special equipment and time-consuming processes are needed.

The method proposed here shows lower hardness and modulus values while indenting on very hard material than those calculated by the method based on Sneddon's solution. This is due to underestimation of the contact area and thus, overestimation of hardness and modulus by the method based the Sneddon's solution. The method proposed here shows almost the same hardness and modulus values when indenting on soft materials as the method based on Sneddon's solution. This is because there is no essential indenter deformation while indenting on soft materials. The hardness and modulus values calculated by this method agree with the finite-element-simulated results by Follstaedt *et al*, except the modulus for the film deposited at –100V substrate bias. No explanation can be found for the one inconsistency at this point.

Finally, it is also possible to integrate this technique into the commercial software for analyzing load-unload/displacement curves. Thus, the real hardness and reduced modulus values can be calculated in seconds, rather than hours or days if done by the finite-element simulation.

4 ACKNOWLEDGEMENT

This work is supported by the Computer Mechanics Laboratory at the University of California at Berkeley. The cathodic-arc carbon films used in this report were manufactured and provided by Dr. O. R. Monteiro at the Lawrence Berkeley National Laboratory.

5 REFERENCE:

1. Sneddon, I. N., 1965, "The relation between load and penetration in the axisymmetric Boussinesq problem for a punch of arbitrary profile", *International Journal of Engineering Science*, No. **3**, pp. 47-57.

2. Pharr, G. M., Oliver, W. C., and Brotzen, F. R., 1992, "On the generality of the relationship among contact stiffness, contact area, and elastic modulus during indentation", *Journal of Material Research*, Vol. **7**, No.**3**, pp. 613-617.

3. Johnson, K. L., 1985, "Contact Mechanics", Cambridge University Press, 37 East 57th Street, New York, NY 10022, USA.

4. Lu, C.-J., Bogy, D. B., and Kaneko, R., 1994, "Nanoindentation hardness tests using a point contact microscope", *Journal of Tribology*, Vol. **116**, pp. 175-180.

5. Lo, R. Y., Bogy, D. B., 1997, "On the measurement of nanohardness and elastic modulus of ultra-thin overcoats: effect of W-doping and annealing on the properties of DLC", Technical Report No. **97-017**, Computer Mechanics Laboratory, Department of Mechanical Engineering, University of California, Berkeley.

6. Monteiro, O. R.; DelplanckeOgletree, M. P.; Lo, R. Y.; Winand, R.; Brown, I., 1997, "Synthesis and characterization of thin films of WCx, produced by mixing W and C plasma streams", *Surface and Coatings Technology*, Vol. **94-5**, No. **1-3**, pp. 220-225.

7. Pharr, G M., Callahan, D. L., McAdams, S. D., Tsui, T. Y., Anders, S., Anders, A., Ager III, J. W., Brown, I. G., Bhatia, C. S., Silva, S. R. P., and Robertson, J.,

1996, “Hardness, elastic modulus, and structure of very hard carbon films produced by cathodic-arc deposition with substrate pulse biasing”, *Applied Physics Letters*, Vol. **68**, No. **6**, pp. 779-81.

8. Follstaedt, D. M., Knapp, J. A., Myers, S. M., Dugger, M., Friedmann, T. A., Sullivan, J. P., Monteiro, O. R., Ager III, J. W., Brown, I. G., and Christenson, T., 1997, “Energetic particle synthesis of metastable layers for superior mechanical properties”, 1997 Fall meeting of Material Research Society.
9. Knapp, J. A., Follstaedt, D. M., Barbour, J. C., Myers, S. M., 1997 “Finite element modeling of nanoindentation for determining the mechanical properties of implanted layers and thin films”, *Nuclear Instruments and Methods in Physics Research*, Sec. **B**, Vol. **127**, pp. 935-939.

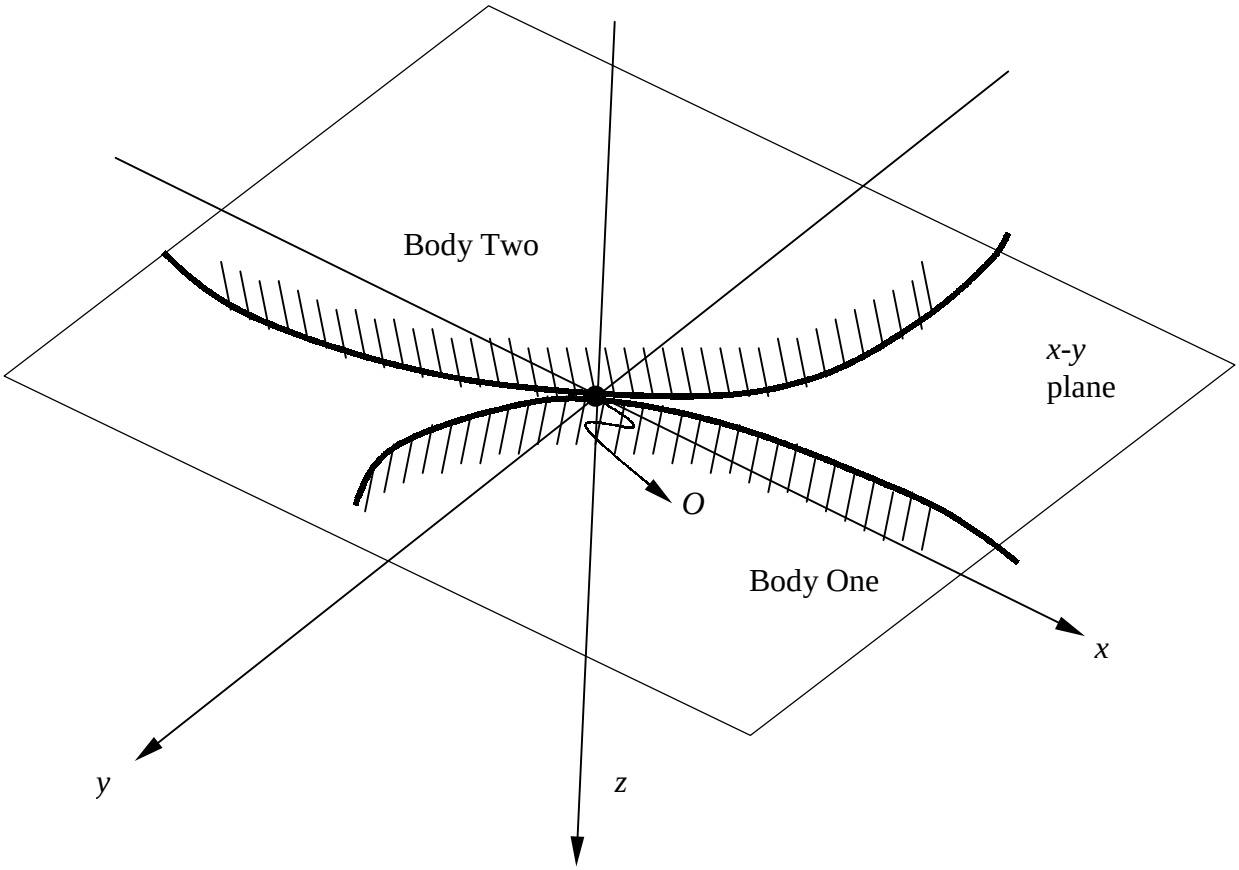

Figure 1: A schematic diagram for two bodies at first contact

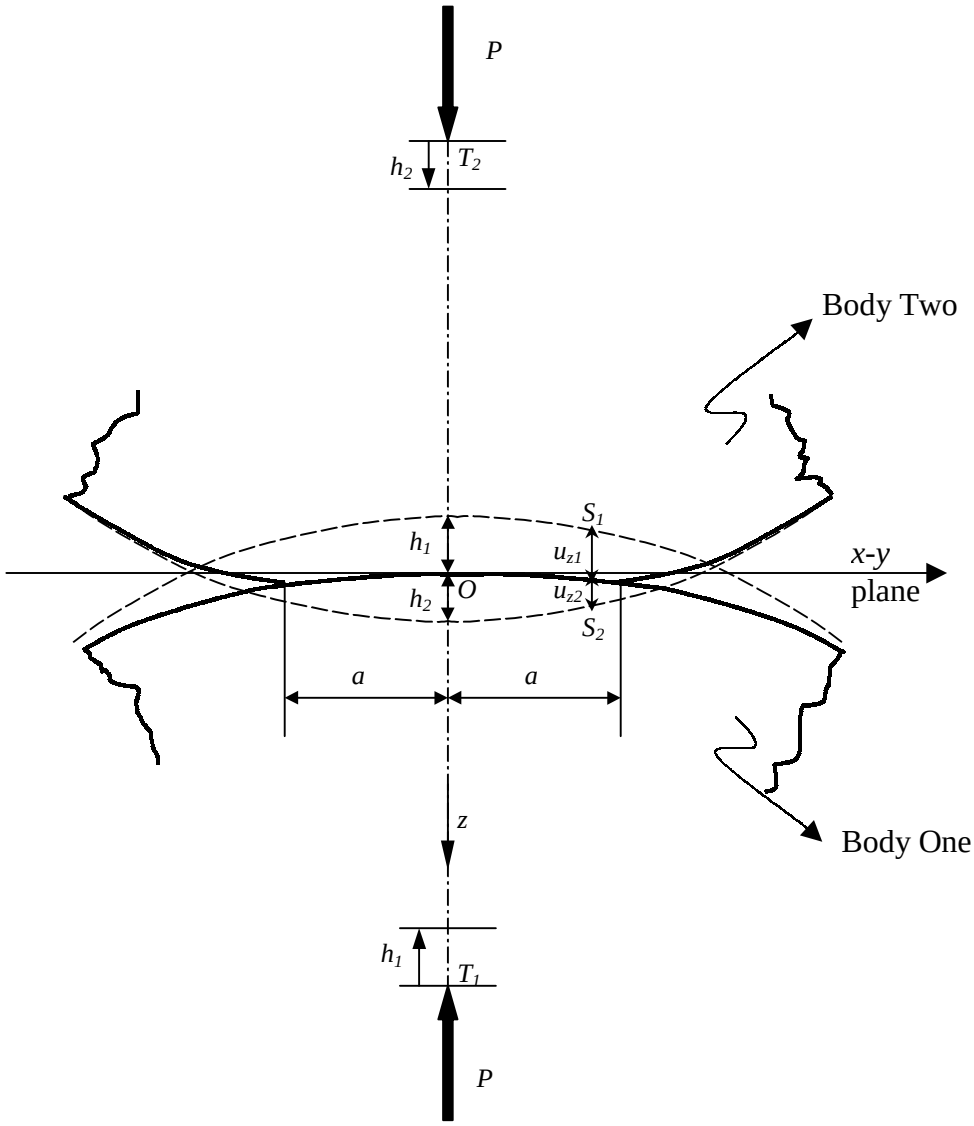

Figure 2: A schematic diagram and the geometry parameters for two solids in contact under a normal load *P*

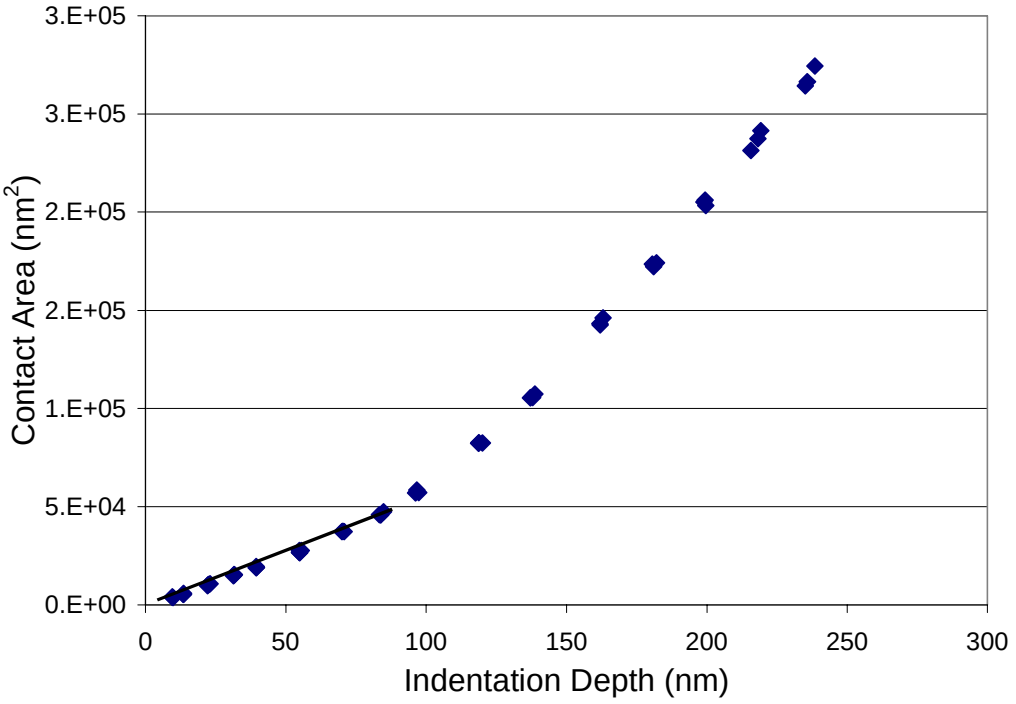

Figure 3: Contact area vs. indentation depth for tip 47 (long range)

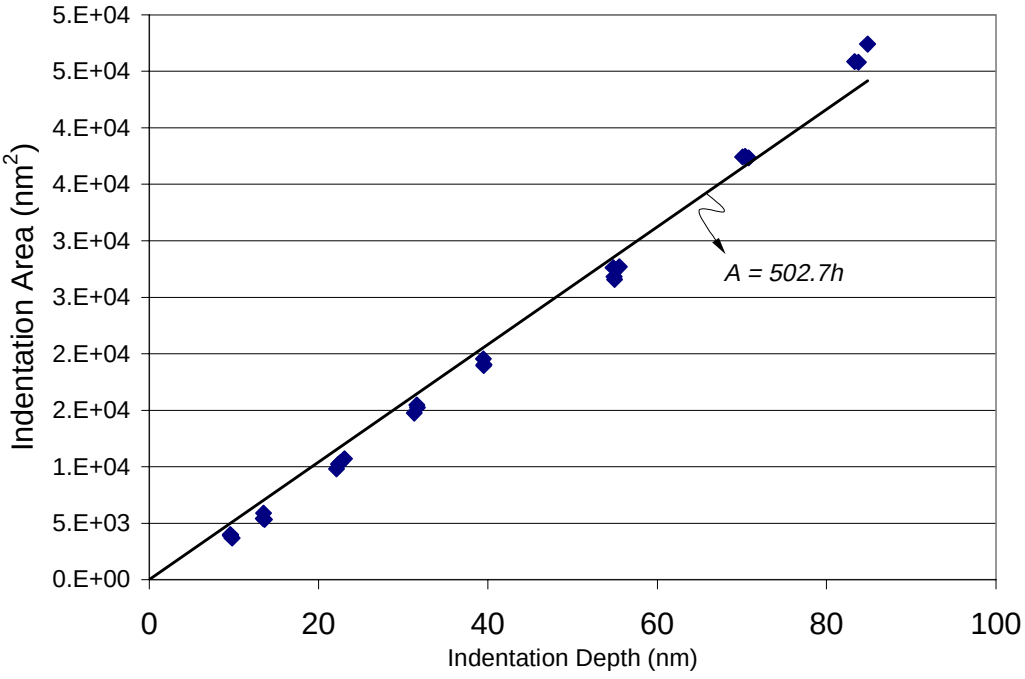

Figure 4: Contact area vs. indentation depth for tip 47 (short range)

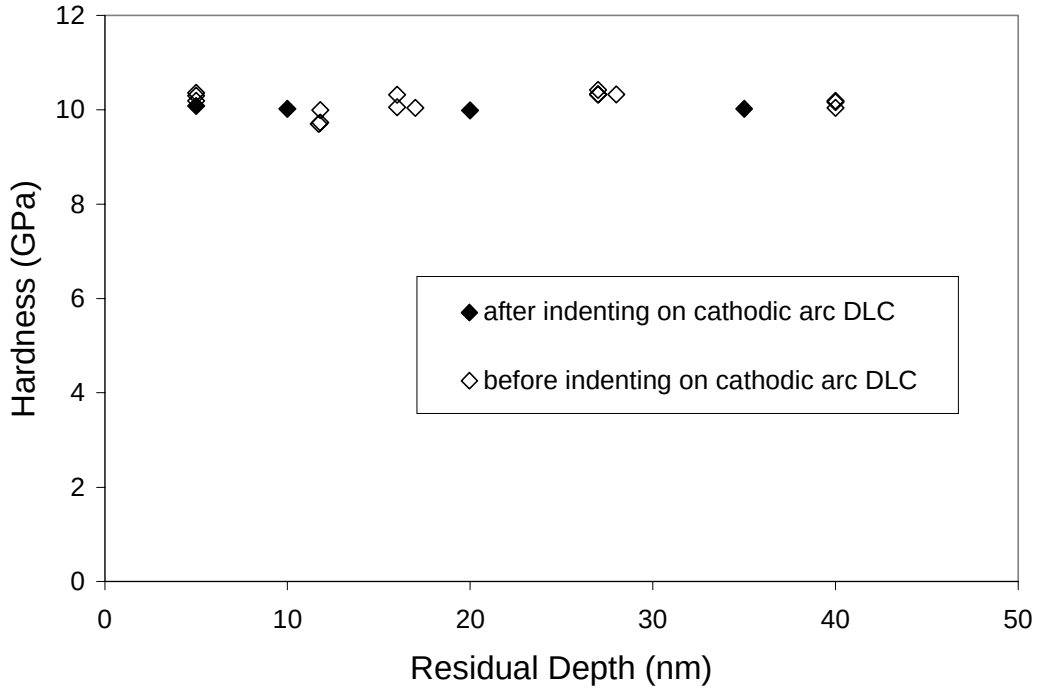

Figure 5: Hardness values calculated by the same tip shape function for tip 47 before and after indenting on a cathodic arc DLC film

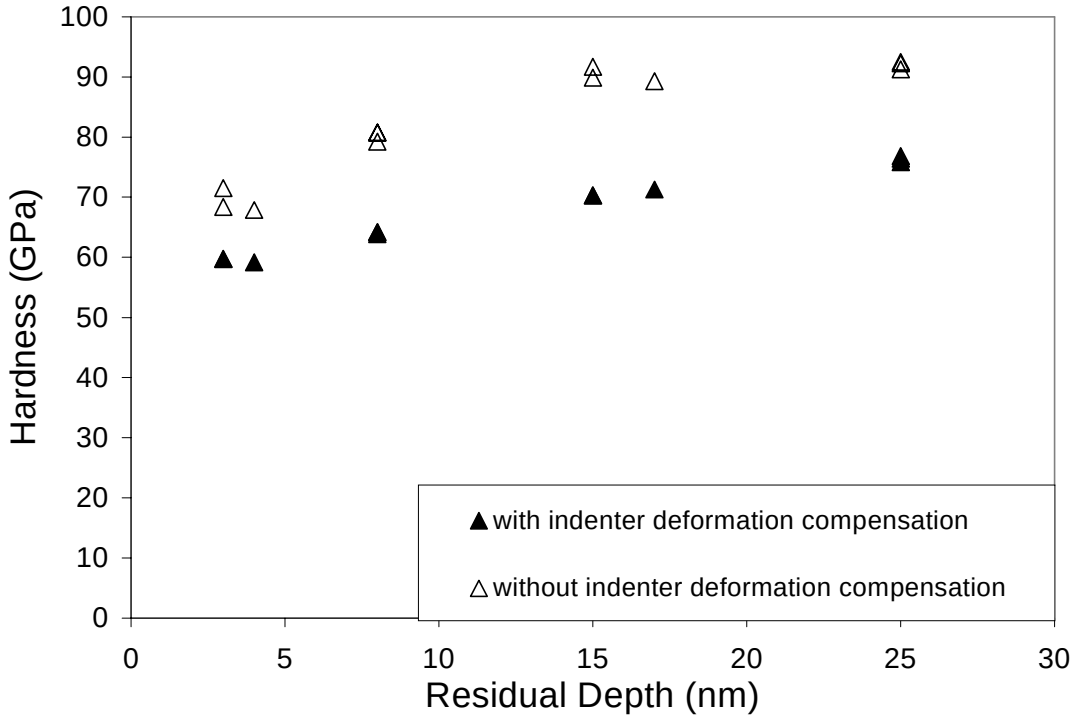

Figure 6: Hardness of the cathodic arc DLC film deposited under –100V substrate bias

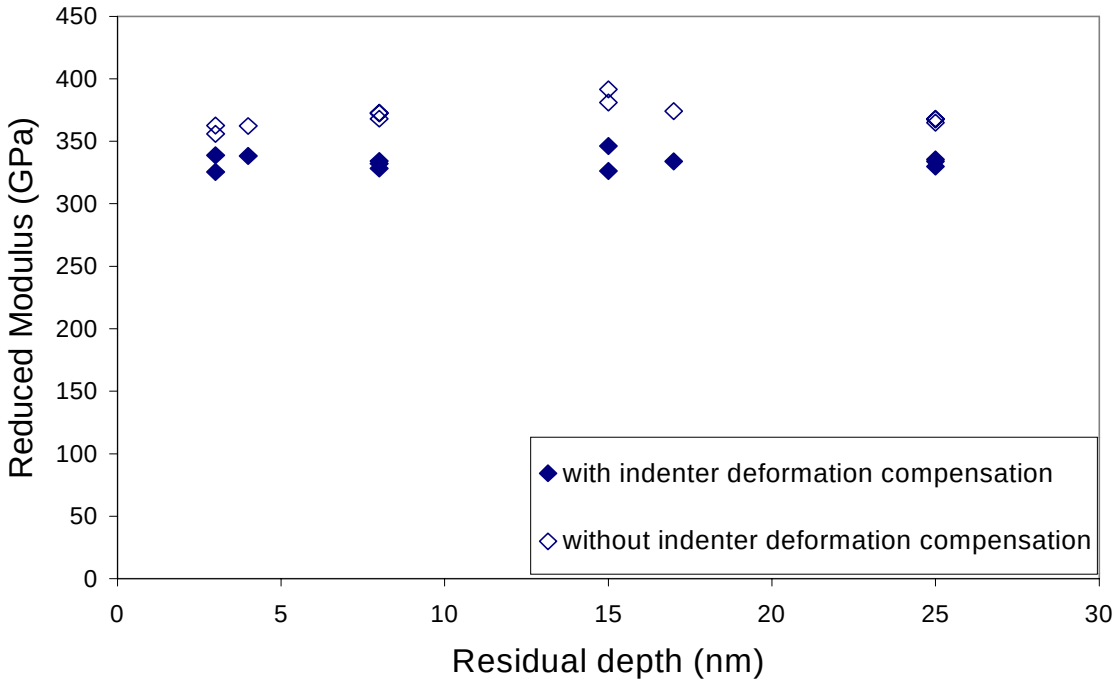

Figure 7: Reduced modulus of the cathodic arc DLC film deposited under –100V substrate bias

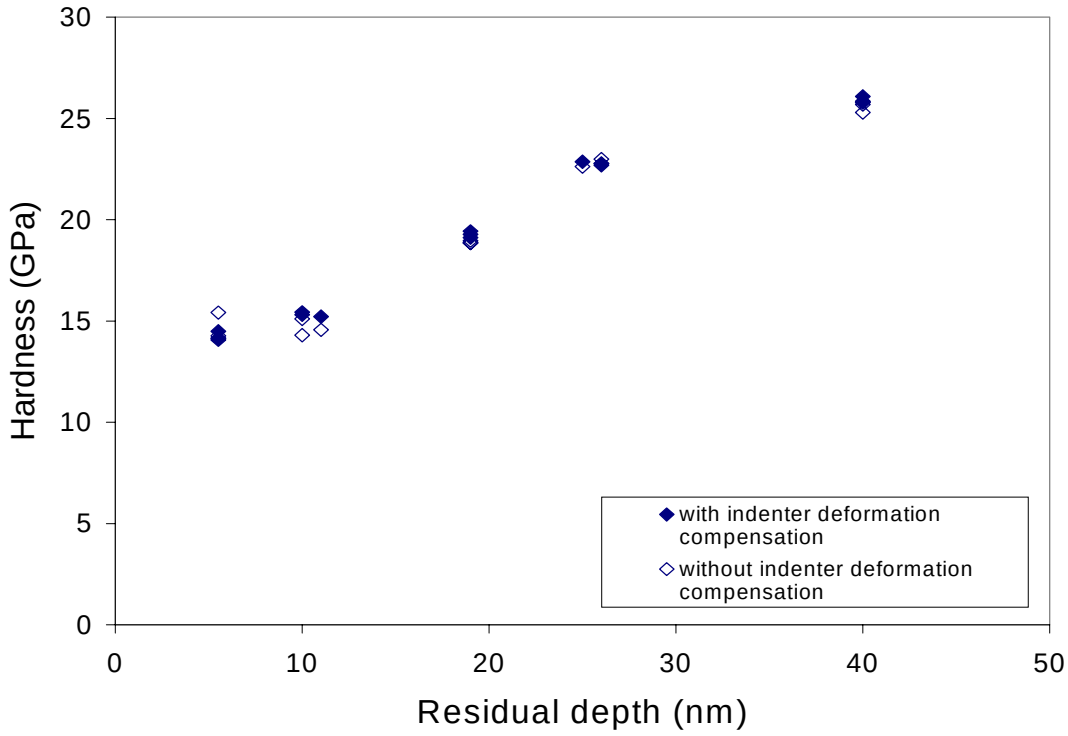

Figure 8: Hardness of the cathodic arc DLC film deposited under –2000V substrate bias

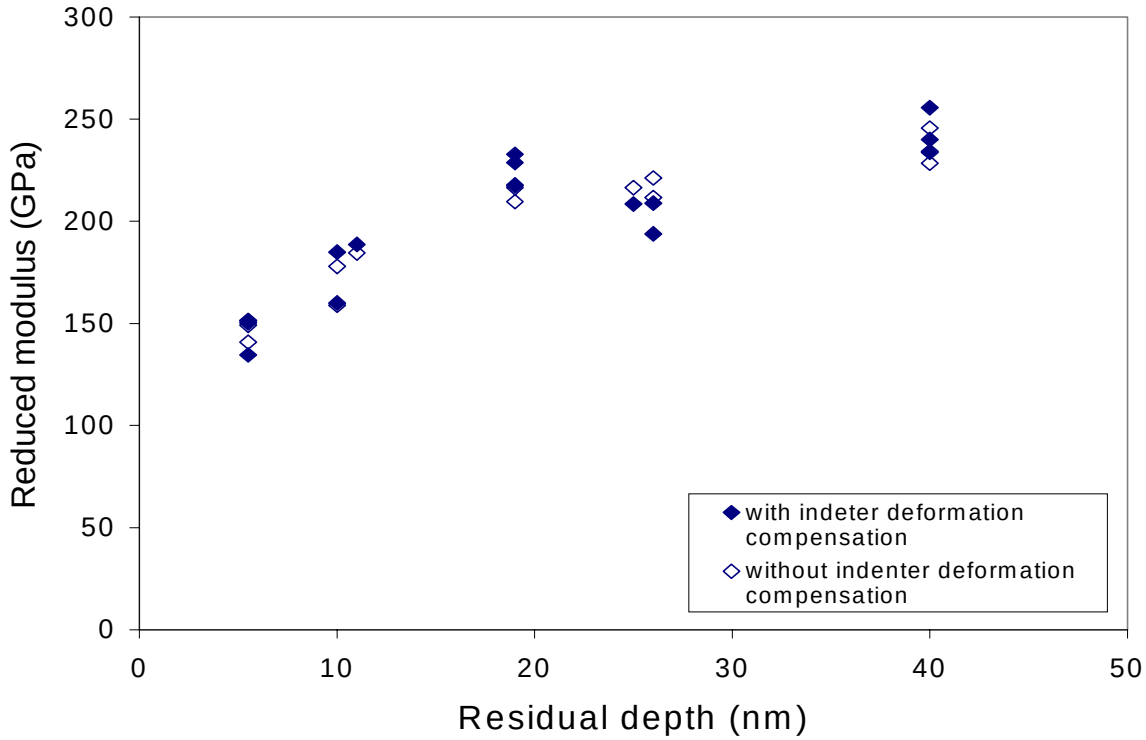

Figure 9: Reduced modulus of the cathodic arc DLC film deposited under –2000V substrate bias